Dalton Transactions

ROYAL SOCIETY OF CHEMISTRY

FRONTIER

View Article Online
View Journal | View Issue

Open Access Article. Published on 15 June 2021. Downloaded on 1/20/2026 11:36:54 AM.
This article is licensed under a Creative Commons Attribution-NonCommercial 3.0 Unported Licence.

Check for updates

Cite this: *Dalton Trans.*, 2021, **50**, 10340

Non-noble MNP@MOF materials: synthesis and applications in heterogeneous catalysis

Nejat Redwan Habib,[a] Esther Asedegbega-Nieto,[b] Abi M. Taddesse[a] and Isabel Diaz *[c]

Received 11th May 2021,
Accepted 11th June 2021

DOI: 10.1039/d1dt01531a

rsc.li/dalton

Transition metals have a long history in heterogeneous catalysis. Noble or precious transition metals have been widely used in this field. The advantage of noble and precious metals is obvious in 'heterogeneous catalysis'. However, the choice of Earth abundant metals is a sustainable alternative due to their abundance and low cost. Preparing these metals in the nanoscale dimension increases their surface area which also increases the catalytic reactions of these materials. Nevertheless, metals are unstable in the nanoparticle form and tend to form aggregates which restrict their applications. Loading metal nanoparticles (MNPs) into highly porous materials is among the many alternatives for combating the unstable nature of the active species. Among porous materials, highly crystalline metal–organic frameworks (MOFs), which are an assembly of metal ions/clusters with organic ligands, are the best candidate. MOFs, on their own, possess catalytic activity derived from the linkers and metal ions or clusters. The catalytic properties of both non-noble metal nanoparticles (MNPs) and MOFs can be improved by loading non-noble MNPs in MOFs yielding MNP@MOF composites with a variety of potential applications, given the synergy and based on the nature of the MNP and MOF. Here, we discussed the synthesis of MNP@MOF materials and the applications of non-noble MNP@MOF materials in heterogeneous catalysis.

[a]*Department of Chemistry, Haramaya University, Haramaya, Ethiopia*
[b]*Departamento de Química Inorgánica y Técnica, Facultad de Ciencias, UNED, c/Senda del Rey no. 9, 28040 Madrid, Spain*
[c]*Instituto de Catálisis y Petroleoquímica, CSIC, c/Marie Curie 2, 28049 Madrid, Spain. E-mail: idiaz@icp.csic.es; Tel: +34 91 585 4785*

1. Introduction

Heterogeneous catalysis based on transition metal nanoparticles is becoming an important field in many industrial

Nejat Redwan Habib

Nejat Redwan Habib received her BSc degree from Hawassa University, Ethiopia, in 2010 with distinction and MSc degree from the University of Gondar in 2013 with distinction and an excellent grade in her MSc thesis. She is an employee of Adama Science and Technology University, Ethiopia, in the position of a lecturer since 2014. She started her PhD study at Haramaya University, Ethiopia, in 2017. She won a pre-doctoral scholarship at the UNED, Spain, on a sustainable chemistry project in 2019–2020. Currently, she is pursuing PhD research work at ICP-CSIC, Spain, on porous materials and their composite synthesis, characterization and application in heterogeneous catalysis.

Esther Asedegbega-Nieto

Esther Asedegbega graduated in chemistry in 2001 and obtained her PhD in chemistry in 2005 from the Universidad Nacional de Educación a Distancia (UNED). In 2006, she had a research contract at the Institute of Catalysis and Petrochemistry. Between 2007 and 2009, she joined the Department of Chemical Engineering and Environmental Technology (Faculty of Chemistry) at the University of Oviedo. At present, she holds a position of an associate professor in the Department of Inorganic and Technical Chemistry (Faculty of Science) at the UNED. Her main line of research includes heterogeneous catalysis in reactions of industrial and environmental relevance.

This journal is © The Royal Society of Chemistry 2021

Open Access Article. Published on 15 June 2021. Downloaded on 1/20/2026 11:36:54 AM.
This article is licensed under a Creative Commons Attribution-NonCommercial 3.0 Unported Licence.

applications.[1–4] The nanosize effect makes these materials exhibit different properties compared to the corresponding bulk materials.[5–8] The exposure of active sites increases due to the high surface area of these materials.[9] Noble and precious metal nanoparticles (MNPs) such as platinum group metals for heterogeneous catalysis have been explored in many research studies.[10–17] It is stated that these materials have unique electronic, chemical, and optical properties depending on the type of noble metal and synthesis conditions.[18–20] On another note, non-noble MNPs have attracted attention in heterogeneous catalysis from the perspective of cost as well as their environmentally friendly nature.[21] Also, by exploring different synthetic conditions and selecting the appropriate non-noble metal, researchers are able to develop non-noble MNP based catalysts which are as efficient as noble MNP based catalysts for heterogeneous catalysis applications.[22]

Besides their high catalytic activities, working with non-noble MNPs is not an easy task due to their thermodynamically unstable nature. Owing to their instability, they tend to form larger aggregates, leading to a decrease in the number of active sites and hence a decrease in catalytic activity due to the lowering of high surface area to volume ratios.[23,24] A multitude of options have been proposed to inhibit such aggregations. The focus has been centered on porous materials used as a support for MNPs to decrease aggregation. Mahugo *et al.* stated that using a support is also important for reducing sintering of MNPs during synthesis or catalytic activity, which increases the reuse of the catalysts as well as protects active sites.[23] Porous silica and carbon, zeolites and metal–organic frameworks (MOFs) have so far been reported as a support for MNPs.[25]

Within the known porous materials, research on MOFs has been growing exponentially.[26,27] MOFs are an assembly of organic ligands with metal ions/clusters.[28] The possibility of using different organic ligands and metal clusters or ions is partly responsible for the vast variety of MOFs designed since their first synthesis in 1999.[28,29] MOFs have intrinsic properties for gas adsorption and separation[30,31] and heterogeneous catalysis[32,33] and are therefore applied in reactions such as photocatalysis[34,35] and biocatalysis[36–39] and even in the field of biomedicine.[40]

Experiments show that combining MNPs with MOFs creates different synergies, which overcome the drawbacks of the individual components and increase the catalytic activities of the composites.[26,41]

This paper highlights the synthesis of MNP@MOF composites with emphasis on the possible synergistic effects derived from combining non-noble MNP@MOFs reported in different works which have already been published so far.

2. MNP@MOF composite synthesis

To date, different synthetic methods have been already explored for MNP@MOF composite synthesis. The synthesis conditions are contingent upon the type of metal and MOF involved as well as the intended applications of the formed composites. Generally, three approaches have been discussed for the synthesis of MNP@MOF composites, as depicted in Fig. 1, wherein different synthetic procedures have been schematized. The first approach called "ship in bottle" consists of placing the preformed MOF into a metal precursor, usually a metal salt solution, for MNP synthesis followed by reducing the metal precursor to its metallic state or the solid state reaction that involves the mixing of the metal salt precursor with the MOF followed by the necessary steps in order to reduce the metal precursor to its metallic form. The second approach known as "bottle around ship" involves the addition of the pre-

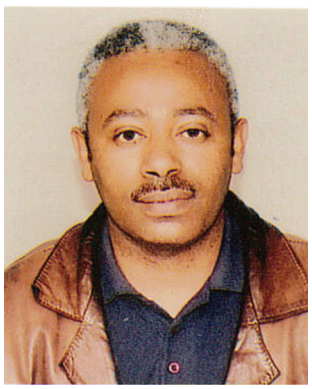

Abi Taddesse

Abi Taddesse received his MSc in inorganic chemistry from Addis Ababa University in 1998 and his PhD degree in soil chemistry from the University of Pretoria in 2008. He was the Dean of the Science Faculty (2008–2012) and the School of Graduate Studies (2012–2015) of Haramaya University. He was a visiting scientist at ICP-CSIC, working on MOF synthesis for various applications between 2015 and 2016. Currently, he is an associate professor of chemistry in the Department of Chemistry, Haramaya University. His research interest is focused on the preparation of advanced materials for various applications such as toxic pollutant degradation, solar cells, and sensors.

Isabel Díaz

Isabel Díaz obtained her PhD in chemistry in 2001 from UAM with the Extraordinary Doctorate Award. She was a Fulbright Fellow at the University of Massachusetts and the University of Minnesota during 2002 and 2003. She was awarded the Royal Spanish Society of Chemistry Prize to Young Researchers in 2007. She is currently a Senior Researcher at ICP-CSIC. She is also Adjunct Professor at the Chemistry Department of Addis Ababa University, Ethiopia. Her main research areas are the synthesis and characterization of zeolites, mesoporous materials and hybrid systems for application in catalysis with special interest in transmission electron microscopy studies.

Open Access Article. Published on 15 June 2021. Downloaded on 1/20/2026 11:36:54 AM.
This article is licensed under a Creative Commons Attribution-NonCommercial 3.0 Unported Licence.

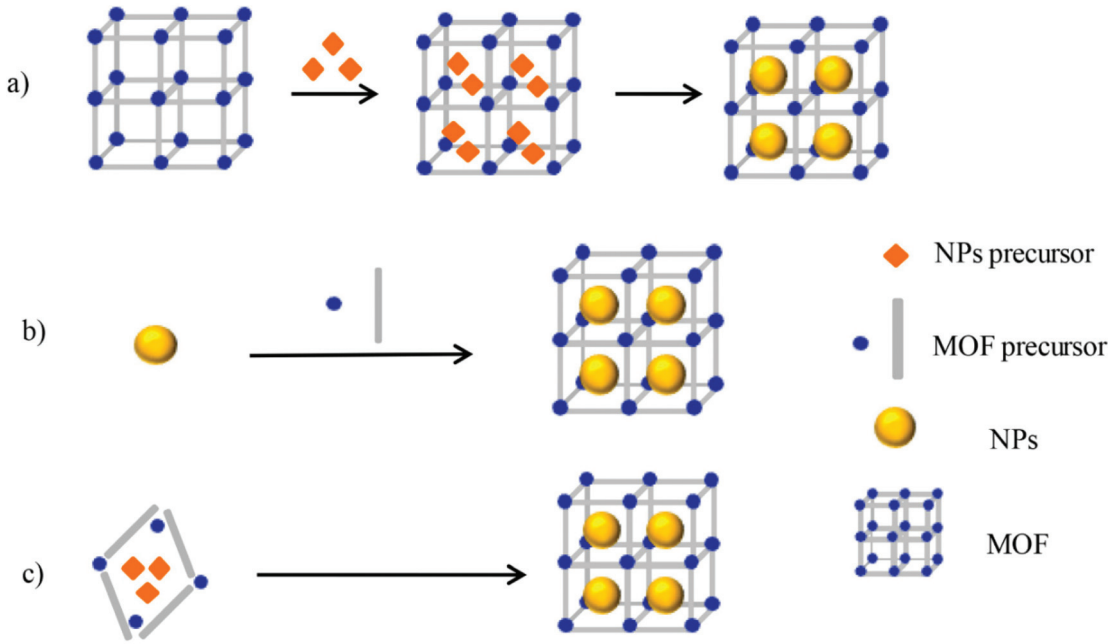

Fig. 1 (a) Ship-in-bottle, (b) bottle-around-ship and (c) one-step synthesis. Reproduced from ref. 43 with permission from MDPI, copyright 2017.

formed MNPs during the synthesis of the MOF.[42] The last approach, the "one step synthesis", as its name implies is based on a one step synthetic procedure whereby both MNP and MOF precursors are mixed resulting in the corresponding composite MNP@MOF.[43]

The ship-in-bottle approach includes procedures such as solid grinding,[44,45] liquid impregnation,[46] double solvent impregnation,[47,48] chemical vapour deposition[49,50] and thermal decomposition.[51,52] These methods generally afford MNPs supported on the MOF surface, though the successful incorporation of MNPs in MOF pores has also been reported.[53] Controlling the guest morphology, location and structure proves to be challenging when using these synthesis routes.[43] This challenge emerges from the microstructure of the MOF, as determined by inner surface characterization, interactions of the MOF with MNPs or the MNP precursor, the pore surface environment of the MOF and the progression of MOF pore wetting and filling.[42] In these methods, to control the location and size of MNPs in the MNP@MOF composite, the following criteria should be considered among many others. These include prior information about the cavity of the MOF with which the metal precursor will be mixed and knowledge of the percent weight loading of MNPs, and the interaction between the MOF cavity and metal precursor should also be studied.[54]

Bottle-around-ship approaches encompass a self-sacrificing template method[48] and emulsion-based interfacial synthesis.[55] Compared to the ship-in-bottle approaches, location and size control of MNPs can be achieved. The main reason for this is that, unlike the ship-in-bottle approaches, these synthesis methods encapsulate the preformed nanoparticles in the MOF precursor materials. However, the demerit is that there is a possibility of affecting the MOF structure when using these methods and not all types of MOFs are suitable for such procedures; so far, UiO-66 and ZIF-8 are mostly reported.[42,43]

Unlike the above stepwise procedures, one-step synthesis is known for its facile and direct approach.[56,57] Kinetic control is necessary since the nucleation and growth of the MOF and MNP are obviously different.[58] In contrast, it would be difficult to obtain MNPs encapsulated in the MOF framework. Surfactants are often applied to obtain small MNPs which also hinder the generation of MOFs.[59]

In any of the three methods, the final question would be whether the MNPs have been successfully and homogenously incorporated into the porous network of the MOF without occupying all available porosity, or avoiding physical mixtures of surface metal phase formation. The challenge in studying MNP@MOF composites is the difficulty of revealing the growth of MNPs in the pores of the MOFs *via* convectional characterization techniques, thus, advanced characterization techniques, including transmission electron microscopy and related spectroscopic techniques may be required to circumvent this challenge.[23,60,61]

3. Synergetic effects of the MNP@MOF composite

Formation of the MNP@MOF composite triggers the corresponding synergy depending on the type of MOF, MNP and the formed composite.[42]

The first synergy which will be explained is surface plasmon, in which photons transform into heat when surface plasmon active materials are simulated by light. This type of synergy is observed on the MNP@MOF composite when MNP

 This journal is © The Royal Society of Chemistry 2021

Open Access Article. Published on 15 June 2021. Downloaded on 1/20/2026 11:36:54 AM.
This article is licensed under a Creative Commons Attribution-NonCommercial 3.0 Unported Licence.

is successfully encapsulated in the MOF framework. Thus, surface plasmon active MNPs, once irradiated by light, heat up the surrounding MOF to discharge the material adsorbed on the framework.[55,62,63] This synergy is mostly reported for adsorption–desorption and drug release applications.[42,54] The surface plasmonic effect of noble MNPs, such as Pt, Pd, Au and so on, is common as reported in different research publications so far.[64–66] For non-noble MNPs, Cu is an example which exhibits a surface plasmonic effect.[67,68]

The second synergy is called size selectivity, which is detected when MNPs are inside the MOF pores. In this synergy the MOF selectively permits the entrance of substrates of smaller size than the MOF's openings but blocks larger substrates, and MNPs inside MOF pores catalyze the reaction.[69–80] This type of synergy is extremely useful especially on the industrial scale for selective catalysis involving organic compounds.[81] A non-noble MNP@MOF with such type of synergy was reported by Nakatsuka *et al.*[82]

The third type of synergy, which is common and appears in most MNP@MOF composites, is MNPs as the active center and the MOF as the stabilizer. This synergy appears irrespective of whether the formed MNPs are outside or inside the framework. This most fundamental synergy has the advantage of preventing aggregation and sintering of MNPs which improves their catalytic activity.[83–89]

The last type of synergistic effect reported is called electron or energy transfer synergy. This synergy is most significant when using a semi-conducting type of MOF, in which light intensity adjustment can generate electrons and lead to energy transfer from the MOF to MNPs or *vice versa*. The ligands and metal ions or clusters of MOFs can affect the catalytic activity of the encapsulated or supported MNPs.[42,90]

In summary, there is sufficient evidence in the literature on the synergy between MNP@MOFs to improve the properties of the composite formed, yet studies to explain this effect in depth are scarce probably due to the difficulty in characterizing such complex systems.

4. Non-noble MNP@MOF composites for heterogeneous catalysis

MOF composite materials are still in the development stage for heterogeneous catalysis. Nonetheless, it has been confirmed so far that MOF composites employed as heterogeneous catalysts have remarkable catalytic actions, reusability and stability.[43] Noble MNP@MOF composites for heterogeneous catalysis have been published in many research publications. Non-noble MNP@MOF composites have recently attracted attention in heterogeneous catalysis. Non-noble MNP@MOF composite catalysts are studied in catalytic pollutant removal applications, such as CO and CO_2 conversions into HCOOH, CH_4, CH_3OH, among others.[53,91] Catalytic organic reactions and H_2 production mostly from chemical hydrides are also experimented with using non-noble MNP@MOF composites.[21,92]

4.1. Catalytic CO_2 reduction

The CO_2 concentration in the environment is constantly increasing. Its implication in the greenhouse effect and long-term climate change is well known. For this reason, CO_2 conversion and treatment have been carried out for decades since its negative environmental impact was discovered. CO_2 conversion into other industrial chemicals such as HCOOH, CH_3OH, CH_4 and cyclic carbonate has been experimented with using many catalytic materials.[91]

CO_2 methanation into CH_4 *via* hydrogenation reaction accounts for its largest hydrogenation product. It is a highly exothermic reaction and can be performed under atmospheric pressure. Noble metal catalysts such as Ru and Rh supported on porous oxides such as SiO_2 and Al_2O_3 are among the noble metal catalysts studied for this reaction.[93,94]. As for non-noble MNP, Ni has been tested on the same support materials.[93] Ni nanoparticles (NPs) supported on the MOF, offer advantages in the perspective of cost and availability compared with noble metals. At the same time, using a highly porous MOF as the support aids in preventing sintering of the active non-noble MNPs and their aggregation.[53]

Zhen *et al.* prepared a *x*Ni@MOF-5 series of active catalysts for CO_2 methanation by the impregnation method (x = % weight of Ni loading). The benchmark catalyst Ni/SiO_2 was used for catalytic comparison with Ni@MOF-5 for methane synthesis.[91] It is stated that the catalytic reaction was carried out in the 180 to 320 °C temperature range to avoid the reverse water gas shift (RWGS) reaction. In the methane production process if the temperature is above 320 °C, the RWGS reaction occurs which results in the formation of CO_2 as a byproduct. With the reference catalyst (Ni/SiO_2), CO_2 conversion is 34% at 280 °C while it was 47.2% under the same condition with Ni@MOF-5. 75.09% CO_2 conversion was obtained with 10Ni@MOF-5 at 320 °C, while the selectivity towards CH_4 was 100%. The specific surface area of 10Ni@MOF-5 is 2961 $m^2\ g^{-1}$ which is very high and it has a pore volume of 1.037 $cm^3\ g^{-1}$, compared to 10Ni/SiO_2 with a specific surface area of 155.6 $m^2\ g^{-1}$ and pore volume of 0.8245. This resulted in high Ni NP dispersion (41.8%) in 10Ni@MOF-5 while it is 33.7% in 10Ni/SiO_2. The reason behind the high catalytic activity of *x*Ni@MOF-5 is the uniform and highly dispersed Ni NPs in MOF-5.[91]

The double solvent impregnation method (DSM) and multiple impregnation (MI) are used to synthesize Ni@MiL-100 (Cr) composites for CO_2 methanation.[53] Here, the study concentrates on the effect of synthesis methods on catalytic methane formation under the same conditions. Ni@MOF synthesized by the DSM, with 20 wt% Ni loading, exhibited higher CO_2 methanation than the corresponding MI synthesized Ni@MIL-101 composites at 300 °C. The possible explanation given is that Ni@MIL-101 synthesized by the DSM has the Ni (111) facet exposed for the catalytic reaction while that exposed for MI synthesized is Ni (200) (Fig. 2). The potential energy barrier for the Ni (111) facet, which is 10.0 kcal mol^{-1}, calcu-

Open Access Article. Published on 15 June 2021. Downloaded on 1/20/2026 11:36:54 AM.
This article is licensed under a Creative Commons Attribution-NonCommercial 3.0 Unported Licence.

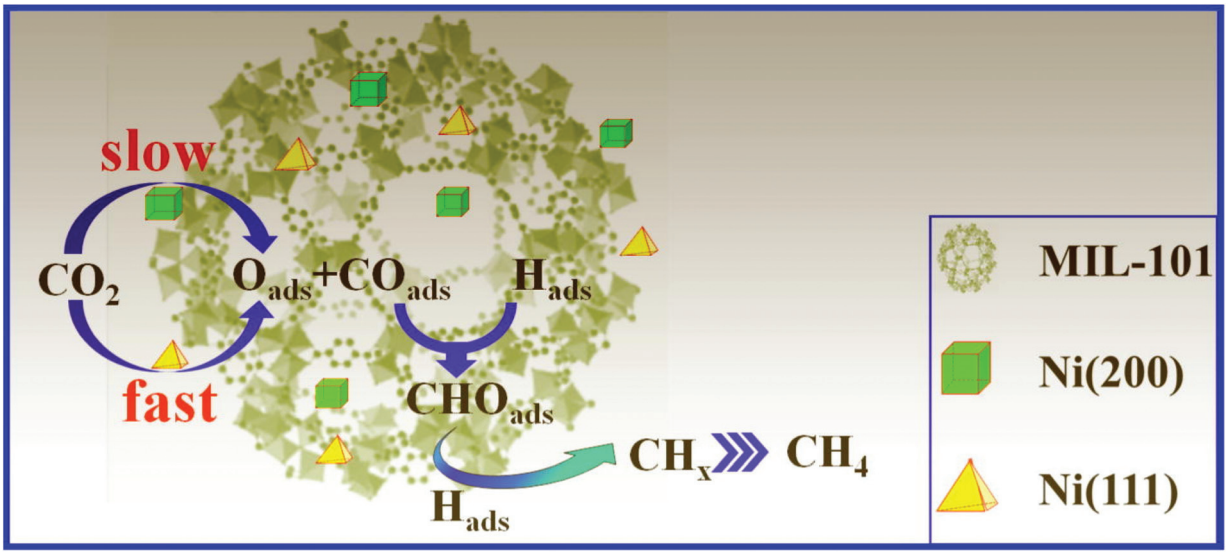

Fig. 2 Ni@MiL-101 for CO_2 methanation over the Ni (200) facet and Ni (111) facet. Reproduced from ref. 53 with permission from Elsevier, copyright 2017.

lated by DFT was lower compared with that of Ni (200) (20.3 kcal mol^{-1}) for the dissociation of CO_2 into adsorbed carbon monoxide and adsorbed oxygen. The dispersion of Ni NPs is 42.3% for 20Ni@MIL-101(Cr) (DSM) and (41.6%) for 20Ni@MIL-101(Cr) (MI). Furthermore, 20Ni@MIL-101(Cr) synthesized by the DSM at a reaction temperature of 280 °C showed a CH_4 TOF (1.2×10^{-3} s^{-1}) value double that of the benchmark catalyst 20Ni/γ-Al_2O_3 at the same temperature.[53]

Cu nanoparticles encapsulated in UiO-66(Zr), Cu nanocrystals (18 nm), have been utilized for the hydrogenation of CO_2 to methanol. CO_2 hydrogenation over Cu@UiO-66 at 175 °C and 10 bar using a H_2/CO_2 molar ratio of 3 showed an initial turnover frequency (TOF) for methanol (MeOH) formation of 3.7×10^{-3} s^{-1}, which is an eight-fold increase in the yield with respect to the reference catalyst Cu/ZnO/Al_2O_3 (0.45×10^{-3} s^{-1}), with 100% selectivity to methanol. UiO-bpy is another UiO-66(Zr) MOF family, which encapsulated ultrafine Cu/ZnO_x to decrease aggregation of Cu NPs and phase separation of ZnO_x and Cu. It was tested for CO_2 hydrogenation with a H_2/CO_2 molar ratio of 3 at 40 bar and 250 °C. CuZn@UiO-bpy showed a space–time yield to MeOH (STY_{MeOH}) of 2.59 g_{MeOH} kg_{Cu}^{-1} h^{-1} at a gas hourly space velocity (GHSV) of 18 000 h^{-1}, which was higher than the value (STY_{MeOH}) of 0.83 g_{MeOH} kg_{Cu}^{-1} h^{-1} obtained with the ternary Cu/ZnO/Al_2O_3 commercial catalyst in a 6/3/1 ratio under the same experimental conditions. CuZn@UiO-bpy shows 100% selectivity and higher stability (>100 h), when compared with the Cu/ZnO/Al_2O_3 catalyst which offers 54.8% methanol selectivity.[95,96]

From the above research works in the catalytic conversion of CO_2, it was observed that the use of MOFs as a support for non-noble MNPs results in high dispersions of catalytically active MNPs compared with a traditional oxide support, such as Al_2O_3 and SiO_2. High dispersion of the catalytically active material in supports favors high reaction performance. This is further evidenced by Zhen *et al.*, on the same non-noble MNPs with different supports, where higher catalytic activity is obtained for Ni@MOF-5 compared with Ni/SiO_2 under the same reaction conditions.[91]

Gutterød *et al.* synthesized Pt NPs encapsulated in UiO-67 (Zr) for methanol formation from CO_2.[97] It is reported that when pressure is increased from 1–8 bar, at 170 °C, a TOF of 0.01 s^{-1} for methanol formation is obtained and selectivity to methanol also increased from 3 to 19% at a 1/6/3 $CO_2/H_2/He$ feed molar ratio.[97] The TOF of methanol formation is higher than that stated for Cu@UiO-66 at 175 °C and 10 bar pressure, as reported by Rungtaweevoranit *et al.*, but the selectivity to methanol is higher with Cu@UiO-66 at 175 °C and 10 bar. However, it is difficult to compare both results, unless it is carried out using the same optimization techniques[96,97].

Table 1 summarizes the catalytic activity of Ni NPs loaded on different types of MOFs for methane formation from CO_2. Generally, Ni NPs are possible substitutes for noble MNPs in MNP@MOF for methane synthesis from CO_2.

4.2. Catalysis for organic compound synthesis

Organic reactions are key procedures that are extensively carried out in industry. Catalytic reactions such as selective

Table 1 Summary of Ni@MOF catalysts for CO_2 methanation

Catalyst	% weight metal loading	Temp. (°C)	CH_4 selectivity	% CO_2 conversion	Ref.
Ni@MOF-5	10	320	100	75	91
Ni@MIL-101 (Cr)	20	300		68.9	53
Ni@MIL-101 (Cr)	20	300	100	100	53
Ni/KIT-6	20	350	100	87.2	98
Ni@UiO-66(Zr)	20	300	100	57.6	99

 This journal is © The Royal Society of Chemistry 2021

Open Access Article. Published on 15 June 2021. Downloaded on 1/20/2026 11:36:54 AM.
This article is licensed under a Creative Commons Attribution-NonCommercial 3.0 Unported Licence.

oxidation of various alcohols are observed as the most fundamental reactions in organic chemistry.[100] Synergistic effects, such as the size selective nature of MOFs and catalytic activity of MNPs make MNP@MOF composite catalysts suitable to participate in highly selective reactions which improve the outcome of these industrial procedures.[43] Noble metals such as Pt and Pd dispersed on high surface area supports are used for many organic compound reactions, such as organic compound hydrogenation.[101]

Here, the focus has been placed on non-noble MNP@MOF composites for hydrogenation and oxidation reactions of organic compounds. Zhou *et al.* stated that supported nanosized nickel particles were found to be effective in hydrogenation reactions.[102] Cu and Ni have been investigated in several research publications as non-noble MNP substitutes in the form of MNP@MOF composites for hydrogenation and oxidation reactions. Table 2 summarizes a list of Cu and Ni NP@MOF composites for hydrogenation and oxidation reactions of organic compounds.

Based on the results summarized in Table 2, various remarks can be made. Supported Ni NPs loaded in the pores of a mesoporous MOF (MesMOF-1) showed high catalytic activity for the hydrogenation of styrene and nitrobenzene. At room temperature, styrene to ethyl benzene conversion was completed in 4 h in methanol medium under H_2 reduction. When nitrobenzene was used as the reactant, the reaction was completed within 15 minutes employing $NaBH_4$ as the hydrogen source in methanol solvent. Even after three cycles of reactions, pure aniline formation was confirmed which is an indication of the stability of the framework.[103]

Cu loaded in UiO-66 MOF, namely Cu(II)@UiO-66-NH_2 and Cu(0)@UiO-66-NH_2 were used for olefin oxidation and hydrogenation. They served as efficient heterogeneous catalysts under mild experimental conditions. At ambient temperature, styrene hydrogenation is completed after 15 minutes of reaction with a quantitative yield. This makes them potential candidates in providing an alternative to the corresponding conventional noble metal catalysts.[104]

4.3. Photocatalysis

The basic photocatalytic process includes absorption of light by the semiconducting medium to form electrons (e^-) and holes (h^+); movement and separation of e^- and h^+ to the surface of the photocatalyst; followed by oxidation reaction by h^+ and reduction reaction by e^-. Therefore, increasing light absorption and creating high separation of e^- and h^+ should be considered when choosing materials as photocatalysts.[34,107]

In MNP@MOF composites, depending on the type of MOF and MNPs, either of the two (MOF or the MNPs) can act as a semiconducting material. The MOF metal ions, clusters or organic linkers can be tailored to obtain a semiconducting MOF. Amino containing ligands are well known for this action. In some types of MNP@MOF composites, photoactive MNPs can be loaded in the pores of the MOF as guest materials. Energy or electron transfer synergy can take place which could be advantageous for the e^- and h^+ separation during photocatalytic reactions. In Fig. 3 a representation of the possible energy or electron transfer can be seen as indicated in a blue bipodal rectangle from the MOF linker to the encapsulated guest which could be an MNP or the metal nodes of the MOF (pictured in red). There is also the possibility of the MOF acting simply as a support and not actively participating in the photocatalytic reactions.[34,108]

There are stability concerns when using MOF materials for photocatalysis especially under moderate acidic and basic con-

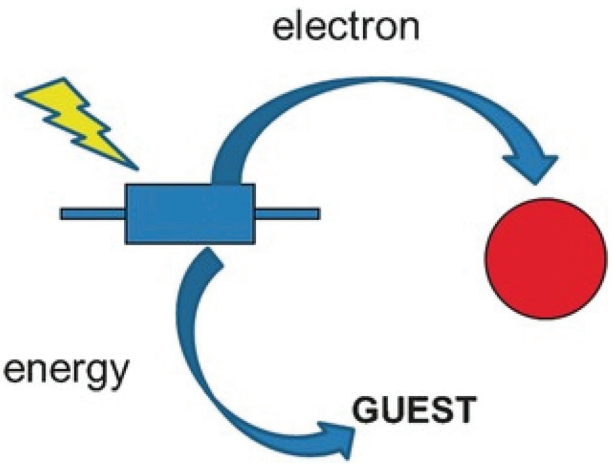

Fig. 3 Energy or electron transfer synergy of MNP@MOF composites. Reproduced from ref. 109 with permission from Wiley, copyright 2016.

Table 2 Cu and Ni NP@MOF catalysts for hydrogenation/oxidation reactions

Catalyst	Type of reaction	Reaction	Reductant/oxidant and solvent	Ref.
Cu(II)/Cu(0)@UiO-66-NH_2	Hydrogenation	Styrene to ethylbenzene	$N_2H_4.H_2O$ in ethanol	104
Ni@MesMOF-1	Hydrogenation	Styrene to ethylbenzene	H_2 gas in methanol	103
Ni@MesMOF-1	Hydrogenation	Nitrobenzene to aniline	$NaBH_4$ in methanol	103
Cu/Cu-BTC	Hydrogenation	Styrene to ethylbenzene	N_2H_4 in H_2O_2	105
Cu/Cu-BDC	Hydrogenation	Styrene to ethylbenzene	N_2H_4 in H_2O_2	105
Cu(II)/Cu(0)@UiO-66-NH_2	Oxidation	Cyclohexene to cyclohexen-1-one and 2-cyclohexen-1-ol	*tert*-Butyl hydroperoxide	104
Cu/MOF-808(Ce)	Oxidation	Cyclohexane to cyclohexanol/cyclohexanone	*tert*-Butyl hydroperoxide	90
Cu/MOF-808(Zr)	Oxidation	Cyclohexane to cyclohexanol/cyclohexanone	*tert*-Butyl hydroperoxide	90
Cu/MOF-808(Ce)	Oxidation	CO to CO_2	O_2	90
Cu/MOF-808(Zr)	Oxidation	CO to CO_2	O_2	90
Ni/NMOF-Ni	Reduction	4-Nitrophenol/4-aminophenol	$NaBH_4$	106

Open Access Article. Published on 15 June 2021. Downloaded on 1/20/2026 11:36:54 AM.
This article is licensed under a Creative Commons Attribution-NonCommercial 3.0 Unported Licence.

ditions. MOFs such as UiO-66(Zr) and zeolitic imidazolate frameworks (ZIFs) are known as stable MOFs under these conditions. The high affinity of zirconium towards oxygen ligands in UiO-66(Zr) and the strong bond of anionic nitrogen containing ligands in ZIFs increase the stability of such MOF families.[34,110]

4.3.1. Photocatalytic degradation of organic pollutants. The environmentally friendly nature of photocatalytic systems offers an advantageous alternative over the conventional organic pollutant degradation methods.[34] Some studies involving MNP@MOF will be discussed in the following paragraphs.

TiO_2@Cu-BTC was synthesized from the titanium(IV) isopropoxide metal precursor by the hydrolysis method under hydrothermal conditions. The photocatalytic reaction of this material was tested for methylene blue (MB) degradation. This material exhibited fast MB degradation compared with the commercial TiO_2-P25 photocatalyst. It is stated that the high porosity of Cu-BTC (BTC = benzene-1,3,5-tricarboxylate) contributed to the high contact surface area which increases the photocatalytic activity compared with the benchmark TiO_2 nanopowder (Degussa P25) catalyst.[111]

The photocatalytic degradation of MB over core–shell Fe_3O_4@MIL-100(Fe), as a Fenton-like catalyst, under solar irradiation is shown in Fig. 4. The study compared the photocatalytic performance of the pure MOF and the composite Fe_3O_4@MIL-100(Fe) counterpart. Here, the MIL-100(Fe) is acting as the photoactive material which means the source of photoinduced e^- and h^+. As described, the Fe_3O_4 is spherical in shape with a particle size of 200 nm obtained by TEM for all samples. It is stated that, irrespective of the MOF thickness (10, 20 and 40 cycles which correspond to 10, 50, and 200 nm respectively), the degradation efficiency of Fe_3O_4@MIL-100(Fe) is higher than that of pure MIL-100(Fe). This is because the presence of a Fe_3O_4 core relayed the photoinduced h^+ of the MOF shell and hence increased the reaction of the e^- with H_2O_2 which results in the formation of hydroxyl radicals. In general, it can be discussed that in this system the production of hydroxyl radicals as a powerful oxidant is enhanced by decreasing e^- and h^+ recombination which increases the photocatalytic degradation of the MB dye. It is confirmed that without the presence of H_2O_2 the MB degradation efficiency is very low which indicates that this catalyst works better as the Fenton-like catalyst. An independent study of the effect of the MOF thickness in the core–shell structure of Fe_3O_4@MIL-100 (Fe) described that the optimal thickness for higher activity was found at 20 cycles. The possible reason given was, the MOF thickness obtained from 20 cycles is not too thick to allow the h^+ formed from the MOF shell to enter the Fe_3O_4 core but thick enough to relay the h^+ so the e^- could react effectively with H_2O_2. Finally, the magnetic nature of the Fe_3O_4@MIL-100(Fe) facilitates the easy separation of the photocatalyst from the solution.[112]

4.3.2. Photocatalytic hydrogen evolution reaction. Depletion of fossil fuel reserves accompanied by climate change is taking place due to the ever-increasing global energy demand. This motivates the need for alternative energy which

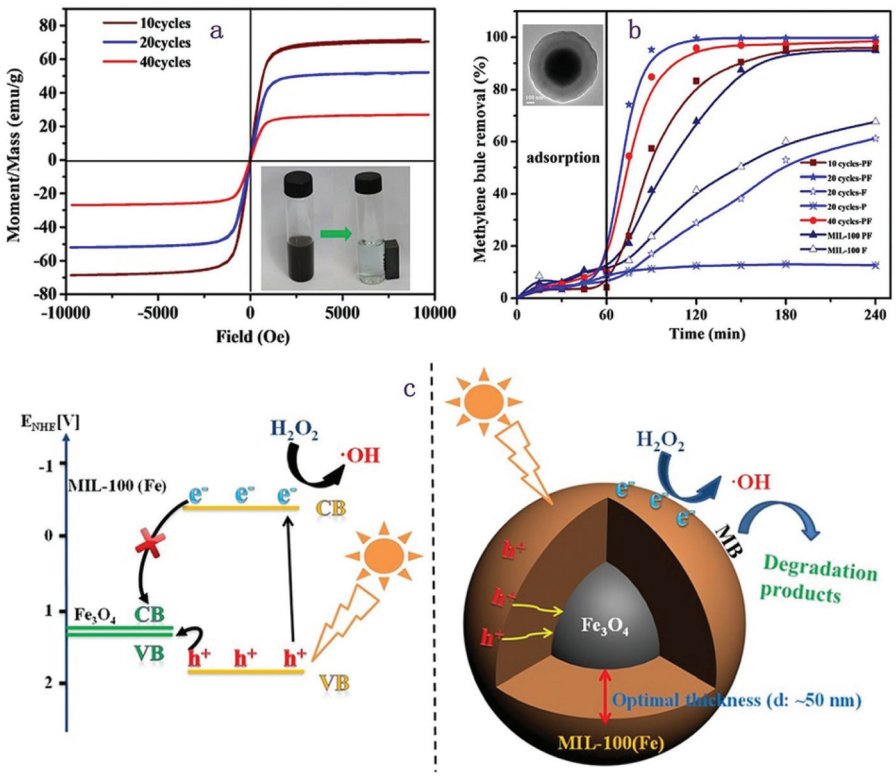

Fig. 4 Proposed mechanism for the photo-Fenton like catalyst. Reproduced from ref. 112 with permission from Wiley, copyright 2015.

Open Access Article. Published on 15 June 2021. Downloaded on 1/20/2026 11:36:54 AM.
This article is licensed under a Creative Commons Attribution-NonCommercial 3.0 Unported Licence.

would depend on environmentally friendly and renewable sources. Intermittent renewable energy sources, such as solar and wind energies, will be a solution to evolve from the fossil-based economy to a renewable energy-based economy. Among different alternatives, H_2 is a particularly attractive energy source, not only because the only combustion product of H_2 is water but also because it has a high gravimetric density which is 120 kJ g^{-1}, comparatively higher than that of petroleum (44 kJ g^{-1}).[113,114]

Obtaining H_2 from water splitting has been researched in depth. It is a sustainable way of obtaining hydrogen compared with other possible methods. In the photocatalytic hydrogen evolution reaction (HER), obtaining H_2 greatly depends on the co-catalyst used in the system which can reduce the overpotential of the HER.[113,114] Pt group metals possess low overpotentials for the HER and have been used as co-catalysts for H_2 production from H_2O.[115] However, it is problematic to scale-up the applications of Pt group catalysts because of their low availability and high cost. It is therefore necessary to find Earth abundant HER co-catalysts that are highly active, stable, low cost and which can show low overpotential for the HER.[109,114,116]

Ni has been studied as a non-noble metal co-catalyst for the HER. Unlike noble MNPs, Ni NPs easily agglomerate giving rise to aggregates, thus leading to low dispersion and hence, low activity. Therefore, to retain the high activity of the Ni NP catalyst, it should be dispersed in highly porous materials with the aim of obtaining well dispersed active sites. Loading Ni in MOF-5 results in highly dispersed Ni nanoparticles, plus the 3D channel MOF-5 structure provides better collection of charge and movement. Therefore, if highly dispersed and small sized MNPs in a MOF is accomplished, then it would be possible to prepare a non-noble metal catalyst (such as Ni NPs) with low overpotential for the HER.[114]

Zhen *et al.*[114] developed Eosin Y (EY) sensitized Ni@MOF-5 and Pt@MOF-5 and compared the H_2 evolution reaction with these catalysts. Fig. 5 shows a mechanism for photocatalytic H_2 evolution over EY sensitized Ni@MOF-5 with triethanolamine (TEOA) as a sacrificial donor, under visible light irradiation. Ni@MOF-5 was prepared by the impregnation method followed by *in situ* chemical reduction methods. A specific area of 2961 m^2 g^{-1} was measured for Ni@MOF-5 which indicates the Ni NPs do not block the framework of the MOF-5 (2973 m^2 g^{-1}), in fact it has a high specific surface area. This is because it was possible to achieve small Ni NPs of only 9 nm. The H_2 generation of EY-MOF-5, EY-Ni-nanoparticles and EY-Ni@MOF-5 was reported as 9.67, 49.9 and 302.2 μmol under 2 h irradiation at $\lambda \geq 420$ nm, respectively. It is explained that there is a possible synergy in EY-Ni@MOF-5 as MOF-5 might drive the photogenerated e^- from excited EY to the hydrogen evolution active site, in this case Ni NPs, which in turn enhances the photocatalytic hydrogen evolution efficiency. It is stated that hydrogen evolution rates of EY-Ni@MOF-5 are comparable to those of EY-Pt-@MOF-5. EY-Ni@MOF-5 showed a little higher H_2 evolution amount in the first 1 h; however, the total H_2 evolution amount is just a little lower than that of EY-Pt-@MOF-5. The maximum H_2 evolution was 302.2 and 353.7 μmol for EY-Ni@MOF-5 and EY-Pt-@MOF-5, respectively, under 2 h irradiation ($\lambda \geq 420$ nm). It is reported that the as-synthesized Ni@MOF has a longer fluorescence lifetime, larger transient photocurrent and shows a low overpotential of −0.37 V. The apparent quantum efficiency (AQE) of EY-Ni@MOF-5 was also reported as 16.7% under 430 nm illumination.[114]

Catalytic hydrogen generation from liquid chemical hydrides, such as aqueous formic acid (HCOOH),[117] ammonia borane (NH_3BH_3)[21,92,118] and hydrazine (N_2H_4)[119] have been reported by MNPs encapsulated in MOF pores. It is stated that, dispersed MNPs inside the MOF could result in enhanced catalytic activity in which the MOF with a high specific surface area and tunable pore size could control the size of MNPs in the confined cavities.[43] Wen *et al.* stated that with the assistance of visible light irradiation an increased hydrogen evol-

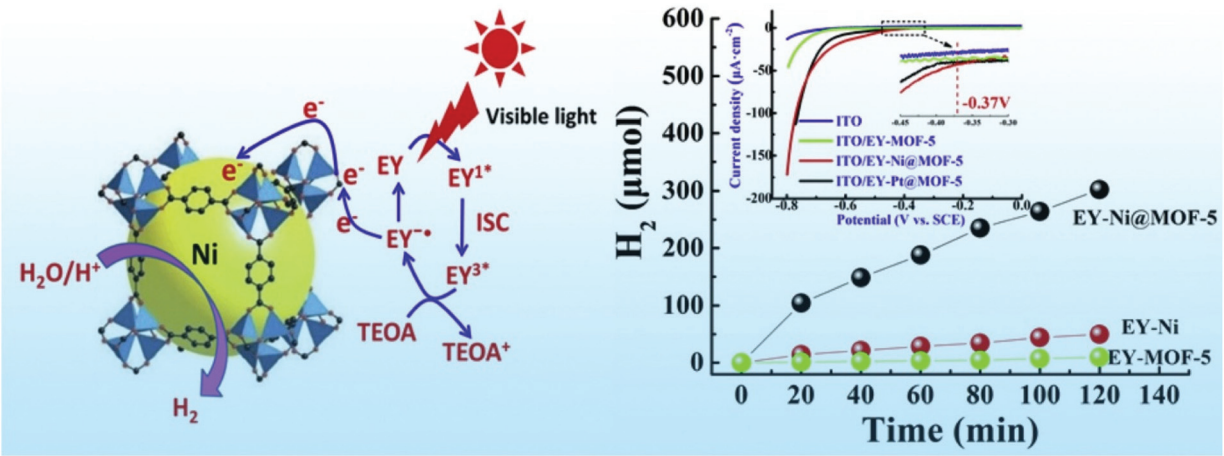

Fig. 5 Photocatalytic H_2 synthesis over EY sensitized Ni@MOF-5 with TEOA. Reproduced from ref. 114 with permission from Elsevier, copyright 2016.

Open Access Article. Published on 15 June 2021. Downloaded on 1/20/2026 11:36:54 AM.
This article is licensed under a Creative Commons Attribution-NonCommercial 3.0 Unported Licence.

Table 3 Non-noble MNP@MOF catalysts for photocatalytic H_2 generation from NH_3BH_3

Catalyst	Chemical hydrides	T (°C)	TOF (h^{-1})	Ref.
CuCo@MIL-101	NH_3BH_3	25	1176	92
FeCo@MIL-101	NH_3BH_3	25	3102	92
NiCo@MIL	NH_3BH_3	25	3048	92
Ni@MIL-101	NH_3BH_3	25	3238	21
Ni@ZIF-8	NH_3BH_3	25	504	118

ution from ammonia borane is obtained with Ni@MIL-101.[21]Table 3 summarizes the catalytic activities of noble-metal free MNP loaded MOFs for hydrogen generation from NH_3BH_3.

4.4. Electrocatalysis

Electrolytic processes such as the oxygen reduction reaction (ORR), oxygen evolution reaction (OER), hydrogen evolution reaction (HER) and carbon dioxide reduction play tremendous roles in energy converting devices such as fuel cells.[120]

MOFs have various characteristics which make them suitable for electrocatalytic reactions. The highly porous nature of MOFs yields high internal surface area, thereby increasing the diffusion of substrates which in turn increases catalytic activity.[121] It is possible to create active sites using MOFs deriving their catalytic activity from metal node sites or from the organic linker side.[122] However, MOFs have poor conductivity when used directly for the electrocatalytic process.[121] So MNPs in the MNP@MOF composite would be a likely solution for the poorly conductive nature of MOFs as well for increasing the stability of the structure.[123] In Fig. 6 some examples of the applications of these materials in electrocatalytic processes are illustrated.

Among many reasons, the sluggish kinetics (high overpotential of the OER and ORR) impede energy converting devices from being practical. The best and most widely used catalysts for the ORR are Pt-based materials.[22,127,128] Nevertheless, as has been discussed throughout this manuscript, there is a need to develop cost-effective catalysts that can readily be efficient for these purposes.[22]

As an alternative to noble metal catalysts, MnO_2@MOF is tested for the ORR. This catalyst shows particularly good catalytic activity for this reaction. The effective catalytic activity of the catalyst is described from the perspective of structure faults and unique electron transfer type during the reaction. The catalytic activity of the active site (MnO_2) depends on its structural faults (*i.e.*, De Wolff faults) and structural defects (*i.e.*, micro-twinning) among the polymorphs, which are known to be promising for the ORR. Also, as for the MOF(Fe) itself, the framework allows easy oxygen diffusion which aids in the catalytic activity. A unique structure is formed for MnO_2@MOF(Fe), in which ε-MnO_2 shows a nanorod morphology with one side strongly holding onto the MOF(Fe) matrix, and the other end protruding which eases the contact with oxygen. All these criteria endow this composite with catalytic activity which is comparable with that of 20% Pt/C. Another quality of this composite is that the electron transfer occurred *via* an apparent-4-electron system (in a two-step 2-electron route). Here is the possible reaction pathway:[22]

$$O_2 + H_2O + 2e^- \rightarrow HO_2^- + OH^- \quad (1)$$

$$HO_2^- + H_2O + 2e^- \rightarrow 3OH^- \quad (2)$$

$$2HO_2^- \rightarrow 2OH^- + O_2 \quad (3)$$

Similarly, in another study, Fe_2O_3 led to enhanced catalytic performance in water oxidation (very low loading of 0.6 wt%) when it was supported on the surface of a non-precious monometallic MOF, Ni-MOF-74. The results were improved with respect to when iron was absent (Ni-MOF-74) or with a catalyst of the same composition but different loading, and the performance was even higher than that of a commercial IrO_2 reference. As a matter of fact, to deliver 10 Am cm^{-2}, an overpotential of 264 mV was needed in contrast to 323 mV in the absence of Fe_2O_3 or 300 mV for the commercial noble metal oxide.[129]

MOFs play an outstanding role not only in encapsulating nanoparticles but can also be used as starting blocks to construct porous carbon materials or for the formation of shell structures. The use of these self-sacrificing templates can favor the presence of single atoms with unique and superior catalytic performance with respect to catalysts with a higher number of atomic aggregates. Among the single atom catalysts reported, those involving non-noble metals such as Fe, Co, Ni, Cu, and Mn, as well as Fe–Co sites have been applied in the electrocatalytic ORR, HER, OER, and CO_2RR. The success of these reactions can be attributed to the use of MOF template materials, such as ZIF-8, ZIF-67, MIL-101-NH_2, and UiO-66-NH_2, for the synthesis of the catalysts.[124] Fig. 6a presents the scheme of the MOF derived single atom electrocatalysts employed in different electrocatalytic reactions as summarized in the above cited review. Other researchers have based their studies on carburization processes of the metal–MOF composite as this can lead to the formation of a graphene shell coating the nanoparticles. In this sense, Xiao *et al.* carried out the carburization of a bimetallic NiMo–MOF to produce electrocatalysts with excellent performance and prolonged duration of 10 h both under acidic and basic conditions[125] (the reaction scheme is depicted in Fig. 6b). The over-potential to reach a current density of 10 mA cm^{-2} was 169 mV for the former and 181 mV for the latter. The synergistic effect of the components (Mo_2C and Ni), graphene coating and porous structure favouring the charge transfer, were key to the remarkable results of these catalysts. More recent studies have shown that for the HER under alkaline media, only 141 mV is needed to attain the current density of 10 mA cm^{-2} when a yolk–shell based on a nitrogen-doped carbon material derived from a MOF is designed.[130] In this referenced work, the yolk was composed of CoP/NC while the shell was made of FeCoP/NC. The obtained structure inhibits the agglomeration of CoP particles which would lead to an increase in the number of accessible active sites. On the other hand, Miner *et al.* produced thin

 This journal is © The Royal Society of Chemistry 2021

Open Access Article. Published on 15 June 2021. Downloaded on 1/20/2026 11:36:54 AM.
This article is licensed under a Creative Commons Attribution-NonCommercial 3.0 Unported Licence.

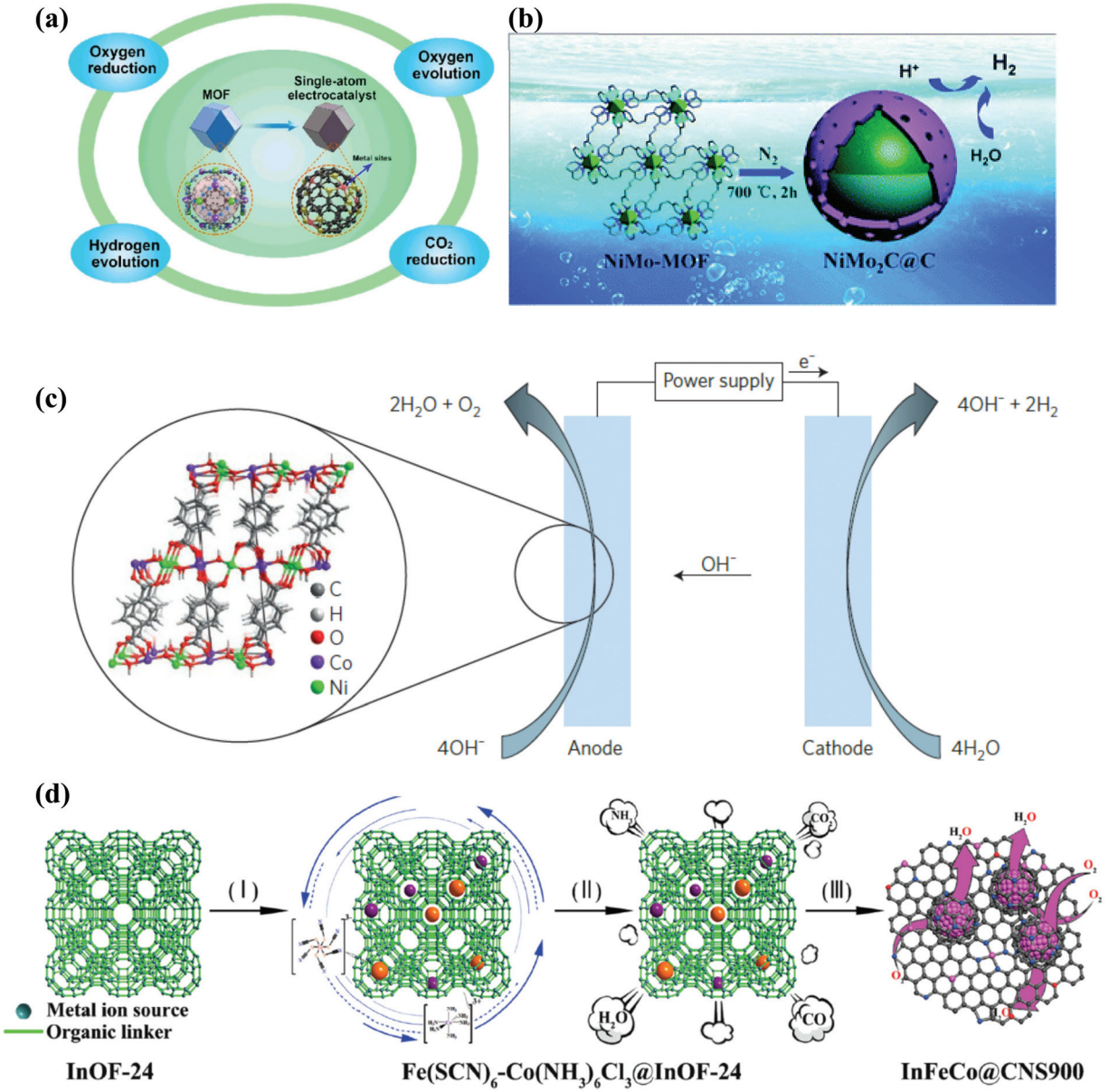

Fig. 6 Successful electrocatalytic applications aided by MOF materials: (a) a MOF based single atom metal material employed in electrocatalysis. Reproduced from ref. 124 with permission from Springer, copyright 2019. (b) Graphene coated MOFs used as OER catalysts. Reproduced from ref. 125 with permission from Royal Society of Chemistry, copyright 2017. (c) Thin sheets of Ni–Co MOFs used as OER catalysts. Reproduced from ref. 126 with permission from Nature, copyright 2016. (d) The ORR performed on hierarchically porous 2-dimensional Fe_4C and FeCo nanoparticles incorporated in N/S-doped carbon support derived from a MOF template. Reproduced from ref. 68 with permission from Royal Society of Chemistry, copyright 2020.

sheets of a Ni–Co-MOF as OER electrocatalysts used under alkaline conditions. As can be viewed in Fig. 6(c), OH^- is oxidized at the anode due to dioxygen while dihydrogen is produced at the cathode upon the reduction of water molecules. Controlling the thickness of the bimetallic MOF was essential for the performance of the generated catalyst.[126] Furthermore, given the importance of synthesizing these ultrathin sheets, various preparation methods are being explored. In a recent study, non-noble metal hierarchically porous 2-dimensional nanosheets were prepared with the aid of a MOF template. This material is based on Fe_4C and FeCo introduced in doped (N/S) carbon materials. The resulting composite (InFeCo@CNS900) is obtained once the lab prepared MOF (InOF-24) has been conveniently calcined (a synthesis scheme can be viewed in Fig. 6(d)). This synthesized composite was employed as an electrocatalyst offering better ORR activity, high diffusion limited current (5.15 mA cm^{-2}) and stability (91.4% after 24 h) compared to a commercial Pt/C catalyst (diffusion limited current of 5.17 mA cm^{-2} and stability equal to 83.4% after 24 h).[68]

Open Access Article. Published on 15 June 2021. Downloaded on 1/20/2026 11:36:54 AM.
This article is licensed under a Creative Commons Attribution-NonCommercial 3.0 Unported Licence.

After all, owing to the advantageous use of these materials, work on exploration of challenges and prospects regarding the development of MOF-derived catalysts is currently in progress.

5. Summary and future perspectives

Literature reports published so far evidenced the possible synergistic effect arising from the integration of MNPs and MOFs. The synergy between MNPs and MOFs is assumed to arise from the plasmonic effect, steric and size selective effects, chemical environment control and electron or energy and substrate transfer. Although advancements have been made in this dynamic field recently, the metals utilized in the preparation of MNP@MOF composites are mostly Pt group metals, which are expensive and less abundant compared to non-noble MNPs. Non-noble MNP loaded MOF systems are becoming valuable alternatives from sustainability and environmental perspectives.

MOFs play a key role in designable structures with clear chemistry. The clear chemistry will be somehow disrupted when additional MNPs are introduced. The possible reasons are the issues related to complex MNPs such as defects and the interactions of MNPs and MOFs. This is the difficulty faced for the future development of these materials. To prepare a size, structure and location controlled MNP@MOF, the properties of MNPs and MOFs independently and their interactions must be studied. The effect of different synthetic conditions such as the additive, solvent and kinetic and thermodynamic parameters have to be experimented with. Detailed investigations for the most part are restricted to the experimental findings of MOFs for different reactions. With respect to the challenge in the characterization of catalysts, increasingly theoretical studies are required apart from the state-of-the art characterization methods currently at hand.

Author contributions

All authors have read and agree to the published version of the manuscript. Conceptualization, N.R.H. and I.D.; investigation, N.R.H.; resources, E.A.N. and I.D.; writing – original draft preparation, N.R.H.; writing – review and editing, E.A.N, A.M.T, and I.D.; supervision, A.M.T. and I.D.; funding acquisition, A.M.T. and I.D.

Conflicts of interest

There are no conflicts to declare.

Acknowledgements

NRH acknowledges the UNED and Fundación Mujeres por África for the scholarship Lear Africa. This work has been funded by the CSIC Project iCOOP-2019 COOPA20376, and 2019AEP076 as well as the Spanish Agency for International Development Cooperation AECID INNOVACION (2020/ACDE/000373). The support from Haramaya University *via* a research project HURG_2020_03_02_75 is duly acknowledged.

References

1 N. Norouzi, M. K. Das, A. J. Richard, A. A. Ibrahim, H. M. El-Kaderi and M. S. El-Shall, *Nanoscale*, 2020, **12**, 19191–19202.
2 B. Lakshminarayana, G. Satyanarayana and C. Subrahmanyam, *ACS Omega*, 2018, **3**, 13065–13072.
3 B. Wei, X. Liu, K. Hua, Y. Deng, H. Wang and Y. Sun, *ACS Appl. Mater. Interfaces*, 2021, **13**, 15113–15121.
4 L. Liu and A. Corma, *Chem. Rev.*, 2018, **118**, 4981–5079.
5 F. Yang, D. Deng, X. Pan, Q. Fu and X. Bao, *Natl. Sci. Rev.*, 2015, **2**, 183–201.
6 X. Zhou, W. Xu, G. Liu, D. Panda and P. Chen, *J. Am. Chem. Soc.*, 2010, **132**, 138–146.
7 O. M. Wilson, M. R. Knecht, J. C. Garcia-Martinez and R. M. Crooks, *J. Am. Chem. Soc.*, 2006, **128**, 4510–4511.
8 P. Suchomel, L. Kvitek, R. Prucek, A. Panacek, A. Halder, S. Vajda and R. Zboril, *Sci. Rep.*, 2018, **8**, 1–11.
9 H. R. Moon, D.-W. Lim and M. P. Suh, *Chem. Soc. Rev.*, 2013, **42**, 1807–1824.
10 M. Liu, L. Zhou, X. Luo, C. Wan and L. Xu, *Catalysts*, 2020, **10**, 1–34.
11 J. A. Kurzman, L. M. Misch and R. Seshadri, *Dalton Trans.*, 2013, **42**, 14653–14667.
12 P. B. Kettler, *Org. Proc. Res. Dev.*, 2003, **7**, 342–354.
13 A. I. Boronin, E. M. Slavinskaya, A. Figueroba, A. I. Stadnichenko, T. Y. Kardash, O. A. Stonkus, E. A. Fedorova, V. v. Muravev, V. A. Svetlichnyi, A. Bruix and K. M. Neyman, *Appl. Catal., B*, 2021, **286**, 119931.
14 B. Han, T. Li, J. Zhang, C. Zeng, H. Matsumoto, Y. Su, B. Qiao and T. Zhang, *Chem. Commun.*, 2020, **56**, 4870–4873.
15 J. Gustafson, O. Balmes, C. Zhang, M. Shipilin, A. Schaefer, B. Hagman, L. R. Merte, N. M. Martin, P. A. Carlsson, M. Jankowski, E. J. Crumlin and E. Lundgren, *ACS Catal.*, 2018, **8**, 4438–4445.
16 M. Qureshi, A. T. Garcia-Esparza, G. Jeantelot, S. Ould-Chikh, A. Aguilar-Tapia, J. L. Hazemann, J. M. Basset, D. Loffreda, T. le Bahers and K. Takanabe, *J. Catal.*, 2019, **376**, 180–190.
17 J. Shan, C. Ye, S. Chen, T. Sun, Y. Jiao, L. Liu, C. Zhu, L. Song, Y. Han, M. Jaroniec, Y. Zhu, Y. Zheng and S.-Z. Qiao, *J. Am. Chem. Soc.*, 2021, **143**, 5201–5211.
18 T. S. Rodrigues, A. G. M. da Silva and P. H. C. Camargo, *J. Mater. Chem. A*, 2019, **7**, 5857–5874.
19 Y. Xu, L. Chen, X. Wang, W. Yao and Q. Zhang, *Nanoscale*, 2015, **7**, 10559–10583.
20 S. Chen, Z. Song, J. Lyu, Y. Guo, B. E. G. Lucier, W. Luo, M. S. Workentin, X. Sun and Y. Huang, *J. Am. Chem. Soc.*, 2020, **142**, 4419–4428.

 This journal is © The Royal Society of Chemistry 2021

Open Access Article. Published on 15 June 2021. Downloaded on 1/20/2026 11:36:54 AM.
This article is licensed under a Creative Commons Attribution-NonCommercial 3.0 Unported Licence.

21 M. Wen, Y. Cui, Y. Kuwahara, K. Mori and H. Yamashita, *ACS Appl. Mater. Interfaces*, 2016, **8**, 21278–21284.
22 H. Wang, F. Yin, B. Chen and G. Li, *J. Mater. Chem. A*, 2015, **3**, 16168–16176.
23 R. Mahugo, A. Mayoral, M. Sánchez-Sánchez and I. Diaz, *Front. Chem.*, 2019, **7**, 686.
24 Q.-L. Zhu and Q. Xu, *Chem*, 2016, **1**, 220–245.
25 D. Xu, H. Lv and B. Liu, *Front. Chem.*, 2018, **6**, 550.
26 R. S. Salama, M. A. Mannaa, H. M. Altass, A. A. Ibrahim and A. E. R. S. Khder, *RSC Adv.*, 2021, **11**, 4318–4326.
27 F. H. Wei, D. Chen, Z. Liang, S. Q. Zhao and Y. Luo, *RSC Adv.*, 2017, **7**, 46520–46528.
28 H. Li, M. Eddaoudi, M. O'Keeffe and O. M. Yaghi, *Nature*, 1999, **402**, 276–279.
29 H. Deng, S. Grunder, K. E. Cordova, C. Valente, H. Furukawa, M. Hmadeh, F. Gandara, A. C. Whalley, Z. Liu, S. Asahina, H. Kazumori, M. O'Keeffe, O. Terasaki, J. F. Stoddart and O. M. Yaghi, *Science*, 2012, **336**, 1018–1023.
30 H. R. Mahdipoor, R. Halladj, E. G. Babakhani, S. Amjad-Iranagh and J. S. Ahari, *RSC Adv.*, 2021, **11**, 5192–5203.
31 B. Li, J. P. Dong, Z. Zhou, R. Wang, L. Y. Wang and S. Q. Zang, *J. Mater. Chem. C*, 2021, **9**, 3429–3439.
32 D. Yang and B. C. Gates, *ACS Catal.*, 2019, **9**, 1779–1798.
33 E. Niknam, F. Panahi, F. Daneshgar, F. Bahrami and A. Khalafi-Nezhad, *ACS Omega*, 2018, **3**, 17135–17144.
34 S.-N. Zhao, G. Wang, D. Poelman and P. van der Voort, *Molecules*, 2018, **23**, 2947.
35 K. Guesh, C. A. D. Caiuby, Á. Mayoral, M. Díaz-García, I. Díaz and M. Sanchez-Sanchez, *Cryst. Growth Des.*, 2017, **17**, 1806–1813.
36 V. Gascón, M. B. Jiménez, R. M. Blanco and M. Sanchez-Sanchez, *Catal. Today*, 2018, **304**, 119–126.
37 V. Gascón, E. Castro-Miguel, M. Díaz-García, R. M. Blanco and M. Sanchez-Sanchez, *J. Chem. Technol. Biotechnol.*, 2017, **92**, 2583–2593.
38 V. Gascón-Pérez, M. B. Jiménez, A. Molina, R. M. Blanco and M. Sánchez-Sánchez, *Catalysts*, 2020, **10**, 1–16.
39 V. Gascón, C. Carucci, M. B. Jiménez, R. M. Blanco, M. Sánchez-Sánchez and E. Magner, *ChemCatChem*, 2017, **9**, 1182–1186.
40 P. Horcajada, R. Gref, T. Baati, P. K. Allan, G. Maurin, P. Couvreur, G. Férey, R. E. Morris and C. Serre, *Chem. Rev.*, 2012, **112**, 1232–1268.
41 X. Gu, Z. Lu, H. Jiang, T. Akita and Q. Xu, *J. Am. Chem. Soc.*, 2011, **133**, 11822–11825.
42 Q. Yang, Q. Xu and H.-L. Jiang, *Chem. Soc. Rev.*, 2017, **46**, 4774–4808.
43 W. Xiang, Y. Zhang, H. Lin and C. Liu, *Molecules*, 2017, **22**, 2103.
44 T. Ishida, M. Nagaoka, T. Akita and M. Haruta, *Chem. – Eur. J.*, 2008, **14**, 8456–8460.
45 H.-L. Jiang, B. Liu, T. Akita, M. Haruta, H. Sakurai and Q. Xu, *J. Am. Chem. Soc.*, 2009, **131**, 11302–11303.
46 K. Leus, P. Concepcion, M. Vandichel, M. Meledina, A. Grirrane, D. Esquivel, S. Turner, D. Poelman, M. Waroquier, V. van Speybroeck, G. van Tendeloo, H. García and P. van der Voort, *RSC Adv.*, 2015, **5**, 22334–22342.
47 C. Hou, Q. Xu, Y. Wang and X. Hu, *RSC Adv.*, 2013, **3**, 19820–19823.
48 Z. Li, R. Yu, J. Huang, Y. Shi, D. Zhang, X. Zhong, D. Wang, Y. Wu and Y. Li, *Nat. Commun.*, 2015, **6**, 8248.
49 S. Hermes, M.-K. Schröter, R. Schmid, L. Khodeir, M. Muhler, A. Tissler, R. W. Fischer and R. A. Fischer, *Angew. Chem., Int. Ed.*, 2005, **44**, 6237–6241.
50 F. Schröder, D. Esken, M. Cokoja, M. W. E. van den Berg, O. I. Lebedev, G. van Tendeloo, B. Walaszek, G. Buntkowsky, H.-H. Limbach, B. Chaudret and R. A. Fischer, *J. Am. Chem. Soc.*, 2008, **130**, 6119–6130.
51 G. Li, H. Kobayashi, K. Kusada, J. M. Taylor, Y. Kubota, K. Kato, M. Takata, T. Yamamoto, S. Matsumura and H. Kitagawa, *Chem. Commun.*, 2014, **50**, 13750–13753.
52 M. Mukoyoshi, H. Kobayashi, K. Kusada, M. Hayashi, T. Yamada, M. Maesato, J. M. Taylor, Y. Kubota, K. Kato, M. Takata, T. Yamamoto, S. Matsumura and H. Kitagawa, *Chem. Commun.*, 2015, **51**, 12463–12466.
53 W. Zhen, F. Gao, B. Tian, P. Ding, Y. Deng, Z. Li, H. Gao and G. Lu, *J. Catal.*, 2017, **348**, 200–211.
54 B. Rungtaweevoranit, Y. Zhao, K. M. Choi and O. M. Yaghi, *Nano Res.*, 2016, **9**, 47–58.
55 L. He, Y. Liu, J. Liu, Y. Xiong, J. Zheng, Y. Liu and Z. Tang, *Angew. Chem., Int. Ed.*, 2013, **52**, 3741–3745.
56 K. Wang, W. Zhao, Q. Zhang, H. Li and F. Zhang, *ACS Omega*, 2020, **5**, 16183–16188.
57 H. Liu, L. Chang, L. Chen and Y. Li, *J. Mater. Chem. A*, 2015, **3**, 8028–8033.
58 H. Liu, L. Chang, C. Bai, L. Chen, R. Luque and Y. Li, *Angew. Chem., Int. Ed.*, 2016, **55**, 5019–5023.
59 L. Chen, R. Luque and Y. Li, *Chem. Soc. Rev.*, 2017, **46**, 4614–4630.
60 C. Li, Q. Zhang and A. Mayoral, *ChemCatChem*, 2020, **12**, 1248–1269.
61 C. Wiktor, M. Meledina, S. Turner, O. I. Lebedev and R. A. Fischer, *J. Mater. Chem. A*, 2017, **5**, 14969–14989.
62 Y. Zhao, N. Kornienko, Z. Liu, C. Zhu, S. Asahina, T.-R. Kuo, W. Bao, C. Xie, A. Hexemer, O. Terasaki, P. Yang and O. M. Yaghi, *J. Am. Chem. Soc.*, 2015, **137**, 2199–2202.
63 L. E. Kreno, N. G. Greeneltch, O. K. Farha, J. T. Hupp and R. P. van Duyne, *Analyst*, 2014, **139**, 4073–4080.
64 P. Verma, K. Yuan, Y. Kuwahara, K. Mori and H. Yamashita, *Appl. Catal., B*, 2018, **223**, 10–15.
65 S. Wieghold, L. Nienhaus, F. L. Knoller, F. F. Schweinberger, J. J. Shepherd, J. W. Lyding, U. Heiz, M. Gruebele and F. Esch, *Phys. Chem. Chem. Phys.*, 2017, **19**, 30570–30577.
66 S. Kunwar, M. Sui, P. Pandey, Z. Gu, S. Pandit and J. Lee, *Sci. Rep.*, 2019, **9**, 1–14.
67 C. L. Huang, G. Kumar, G. D. Sharma and F. C. Chen, *Appl. Phys. Lett.*, 2020, **116**, 253302.

Open Access Article. Published on 15 June 2021. Downloaded on 1/20/2026 11:36:54 AM.
This article is licensed under a Creative Commons Attribution-NonCommercial 3.0 Unported Licence.

68 Q. Huang, Y. Guo, X. Wang, L. Chai, J. Ding, L. Zhong, T. T. Li, Y. Hu, J. Qian and S. Huang, *Nanoscale*, 2020, **12**, 10019–10025.
69 Z. Guo, C. Xiao, R. v. Maligal-Ganesh, L. Zhou, T. W. Goh, X. Li, D. Tesfagaber, A. Thiel and W. Huang, *ACS Catal.*, 2014, **4**, 1340–1348.
70 G. Lu, S. Li, Z. Guo, O. K. Farha, B. G. Hauser, X. Qi, Y. Wang, X. Wang, S. Han, X. Liu, J. S. DuChene, H. Zhang, Q. Zhang, X. Chen, J. Ma, S. C. J. Loo, W. D. Wei, Y. Yang, J. T. Hupp and F. Huo, *Nat. Chem.*, 2012, **4**, 310–316.
71 J. Zhou, P. Wang, C. Wang, Y. T. Goh, Z. Fang, P. B. Messersmith and H. Duan, *ACS Nano*, 2015, **9**, 6951–6960.
72 P. Wang, J. Zhao, X. Li, Y. Yang, Q. Yang and C. Li, *Chem. Commun.*, 2013, **49**, 3330–3332.
73 C.-H. Kuo, Y. Tang, L.-Y. Chou, B. T. Sneed, C. N. Brodsky, Z. Zhao and C.-K. Tsung, *J. Am. Chem. Soc.*, 2012, **134**, 14345–14348.
74 Y. Yang, F. Wang, Q. Yang, Y. Hu, H. Yan, Y.-Z. Chen, H. Liu, G. Zhang, J. Lu, H.-L. Jiang and H. Xu, *ACS Appl. Mater. Interfaces*, 2014, **6**, 18163–18171.
75 B. Xi, Y. C. Tan and H. C. Zeng, *Chem. Mater.*, 2016, **28**, 326–336.
76 Z. Xu, W. Zhang, J. Weng, W. Huang, D. Tian and F. Huo, *Nano Res.*, 2016, **9**, 158–134.
77 Q. Yang, Q. Xu, S.-H. Yu and H.-L. Jiang, *Angew. Chem., Int. Ed.*, 2016, **55**, 3685–3689.
78 C. J. Stephenson, J. T. Hupp and O. K. Farha, *Inorg. Chem.*, 2016, **55**, 1361–1363.
79 C. J. Stephenson, J. T. Hupp and O. K. Farha, *Inorg. Chem. Front.*, 2015, **2**, 448–452.
80 S. Aguado, S. El-Jamal, F. Meunier, J. Canivet and D. Farrusseng, *Chem. Commun.*, 2016, **52**, 7161–7163.
81 K. Wang, W. Zhao, Q. Zhang, H. Li and F. Zhang, *ACS Omega*, 2020, **5**, 16183–16188.
82 K. Nakatsuka, T. Yoshii, Y. Kuwahara, K. Mori and H. Yamashita, *Chem. – Eur. J.*, 2018, **24**, 898–905.
83 S. Gao, N. Zhao, M. Shu and S. Che, *Appl. Catal., A*, 2010, **388**, 196–201.
84 H. Li, Z. Zhu, F. Zhang, S. Xie, H. Li, P. Li and X. Zhou, *ACS Catal.*, 2011, **1**, 1604–1612.
85 M. Yadav and Q. Xu, *Chem. Commun.*, 2013, **49**, 3327–3329.
86 Y. Huang, T. Ma, P. Huang, D. Wu, Z. Lin and R. Cao, *ChemCatChem*, 2013, **5**, 1877–1883.
87 C. Hou, G. Zhao, Y. Ji, Z. Niu, D. Wang and Y. Li, *Nano Res.*, 2014, **7**, 1364–1369.
88 V. Pascanu, F. Carson, M. V. Solano, J. Su, X. Zou, M. J. Johansson and B. Martín-Matute, *Chem. – Eur. J.*, 2016, **22**, 3729–3737.
89 F. Carson, V. Pascanu, A. Bermejo Gómez, Y. Zhang, A. E. Platero-Prats, X. Zou and B. Martín-Matute, *Chem. – Eur. J.*, 2015, **21**, 10896–10902.
90 X. He, B. G. Looker, K. T. Dinh, A. W. Stubbs, T. Chen, R. J. Meyer, P. Serna, Y. Román-Leshkov, K. M. Lancaster and M. Dincă, *ACS Catal.*, 2020, **10**, 7820–7825.
91 W. Zhen, B. Li, G. Lu and J. Ma, *Chem. Commun.*, 2015, **51**, 1728–1731.
92 P. Liu, X. Gu, K. Kang, H. Zhang, J. Cheng and H. Su, *ACS Appl. Mater. Interfaces*, 2017, **9**, 10759–10767.
93 C. Kim, S. Hyeon, J. Lee, W. D. Kim, D. C. Lee, J. Kim and H. Lee, *Nat. Commun.*, 2018, **9**, 1–8.
94 A. Karelovic and P. Ruiz, *Appl. Catal., B*, 2012, **113–114**, 237–249.
95 B. An, J. Zhang, K. Cheng, P. Ji, C. Wang and W. Lin, *J. Am. Chem. Soc.*, 2017, **139**, 3834–3840.
96 B. Rungtaweevoranit, J. Baek, J. R. Araujo, B. S. Archanjo, K. M. Choi, O. M. Yaghi and G. A. Somorjai, *Nano Lett.*, 2016, **16**, 7645–7649.
97 E. S. Gutterød, A. Lazzarini, T. Fjermestad, G. Kaur, M. Manzoli, S. Bordiga, S. Svelle, K. P. Lillerud, E. Skúlason, S. Øien-ØDegaard, A. Nova and U. Olsbye, *J. Am. Chem. Soc.*, 2020, **142**, 999–1009.
98 H. Cao, W. Wang, T. Cui, H. Wang, G. Zhu and X. Ren, *Energies*, 2020, **13**, 2235.
99 Z. W. Zhao, X. Zhou, Y. N. Liu, C. C. Shen, C. Z. Yuan, Y. F. Jiang, S. J. Zhao, L. B. Ma, T. Y. Cheang and A. W. Xu, *Catal. Sci. Technol.*, 2018, **8**, 3160–3165.
100 C. Xu, C. Zhang, H. Li, X. Zhao, L. Song and X. Li, *Catal. Surv. Asia*, 2016, **20**, 13–22.
101 S. Navalón, M. Álvaro, A. Dhakshinamoorthy and H. García, *Molecules*, 2019, **24**, 3050.
102 L. Zhou, M. Wen, Q. Wu and D. Wu, *Dalton Trans.*, 2014, **43**, 7924–7929.
103 Y. K. Park, S. B. Choi, H. J. Nam, D.-Y. Jung, H. C. Ahn, K. Choi, H. Furukawa and J. Kim, *Chem. Commun.*, 2010, **46**, 3086.
104 J.-C. Wang, Y.-H. Hu, G.-J. Chen and Y.-B. Dong, *Chem. Commun.*, 2016, **52**, 13116–13119.
105 A. K. Kar and R. Srivastava, *New J. Chem.*, 2018, **42**, 9557–9567.
106 T. Guo, C. Wang, N. Zhang, Y. Zhang, T. Chen, X. Xing, Z. Lu and L. Wen, *Cryst. Growth Des.*, 2020, **20**, 6217–6225.
107 L. Shen, R. Liang and L. Wu, *Chin. J. Catal.*, 2015, **36**, 2071–2088.
108 X. Deng, Z. Li and H. García, *Chem. – Eur. J.*, 2017, **23**, 11189–11209.
109 A. Dhakshinamoorthy, A. M. Asiri and H. García, *Angew. Chem., Int. Ed.*, 2016, **55**, 5414–5445.
110 Z. Jin and H. Yang, *Nanoscale Res. Lett.*, 2017, **12**, 539.
111 N. T. Binh, P. T. Thu, N. T. H. Le, D. M. Tien, H. T. Khuyen, L. T. K. Giang, N. T. Huong and T. D. Lam, *Int. J. Green Nanotechnol.*, 2015, **12**, 447–455.
112 H. Zhao, L. Qian, H. Lv, Y. Wang and G. Zhao, *ChemCatChem*, 2015, **7**, 4148–4155.
113 F. Song, W. Li and Y. Sun, *Inorganics*, 2017, **5**, 40.
114 W. Zhen, J. Ma and G. Lu, *Appl. Catal., B*, 2016, **190**, 12–25.
115 L. Zhang, K. Doyle-Davis and X. Sun, *Energy Environ. Sci.*, 2019, **12**, 492–517.
116 X.-J. Kong, Z. Lin, Z.-M. Zhang, T. Zhang and W. Lin, *Angew. Chem., Int. Ed.*, 2016, **55**, 6411–6416.
117 F. Ke, L. Wang and J. Zhu, *Nanoscale*, 2015, **7**, 8321–8325.

 This journal is © The Royal Society of Chemistry 2021

Open Access Article. Published on 15 June 2021. Downloaded on 1/20/2026 11:36:54 AM.
This article is licensed under a Creative Commons Attribution-NonCommercial 3.0 Unported Licence.

118 P.-Z. Li, K. Aranishi and Q. Xu, *Chem. Commun.*, 2012, **48**, 3173–3175.
119 Z. Zhang, S. Zhang, Q. Yao, X. Chen and Z. H. Lu, *Inorg. Chem.*, 2017, **56**, 11938–11945.
120 Y. Luo and N. Alonso-Vante, in *SPR Electrochemistry*, ed. C. Banks and S. McIntosh, RSC Chemistry, London, 2017, vol. 14, pp. 194–256.
121 Z. Song, N. Cheng, A. Lushington and X. Sun, *Catalysts*, 2016, **6**, 116.
122 C. Caratelli, J. Hajek, F. G. Cirujano, M. Waroquier, F. X. Llabrés i Xamena and V. van Speybroeck, *J. Catal.*, 2017, **352**, 401–414.
123 A. Kim, N. Muthuchamy, C. Yoon, S. Joo and K. Park, *Nanomaterials*, 2018, **8**, 138.
124 T. Sun, L. Xu, D. Wang and Y. Li, *Nano Res.*, 2019, **12**, 2067–2080.
125 X. Li, L. Yang, T. Su, X. Wang, C. Sun and Z. Su, *J. Mater. Chem. A*, 2017, **5**, 5000–5006.
126 E. M. Miner and M. Dinca, *Nat. Energy*, 2016, **1**, 1–2.
127 N. Cheng, L. Zhang, K. Doyle-Davis and X. Sun, *Electrochem. Energy Rev.*, 2019, **2**, 539–573.
128 Z. Song, L. Zhang, K. Doyle-Davis, X. Fu, J. L. Luo and X. Sun, *Adv. Energy Mater.*, 2020, **10**, 1–42.
129 Z. Gao, Z. W. Yu, F. Q. Liu, Y. Yu, X. M. Su, L. Wang, Z. Z. Xu, Y. L. Yang, G. R. Wu, X. F. Feng and F. Luo, *Inorg. Chem.*, 2019, **58**, 11500–11507.
130 J. Shi, F. Qiu, W. Yuan, M. Guo and Z. H. Lu, *Chem. Eng. J.*, 2021, **403**, 126312.